

# A Novel Pleckstrin Homology Domain-containing Protein Enhances Insulin-stimulated Akt Phosphorylation and GLUT4 Translocation in Adipocytes\*

Received for publication, May 20, 2010, and in revised form, June 18, 2010. Published, JBC Papers in Press, June 28, 2010, DOI 10.1074/jbc.M110.146886

Qiong L. Zhou<sup>‡</sup>, Zhen Y. Jiang<sup>§1</sup>, Allan S. Mabardy<sup>‡</sup>, Claudia M. Del Campo<sup>‡</sup>, David G. Lambright<sup>‡</sup>, John Holik<sup>¶</sup>, Kevin E. Fogarty<sup>‡</sup>, Juerg Straubhaar<sup>‡</sup>, Sarah Nicoloro<sup>‡</sup>, Anil Chawla<sup>‡</sup>, and Michael P. Czech<sup>‡2</sup>

From the <sup>‡</sup>Program in Molecular Medicine and <sup>¶</sup>Department of Biochemistry and Molecular Pharmacology, University of Massachusetts Medical School, Worcester, Massachusetts 01605 and the <sup>§</sup>Metabolic Signaling and Disease Program, Diabetes and Obesity Research Center, Sanford/Burnham Medical Research Institute at Lake Nona, Orlando, Florida 32827

Protein kinase B/Akt protein kinases control an array of diverse functions, including cell growth, survival, proliferation, and metabolism. We report here the identification of pleckstrin homology-like domain family B member 1 (PHLDB1) as an insulin-responsive protein that enhances Akt activation. PHLDB1 contains a pleckstrin homology domain, which we show binds phosphatidylinositol PI(3,4)P<sub>2</sub>, PI(3,5)P<sub>2</sub>, and PI(3,4,5)P<sub>3</sub>, as well as a Forkhead-associated domain and coiled coil regions. PHLDB1 expression is increased during adipocyte differentiation, and it is abundant in many mouse tissues. Both endogenous and HA- or GFP-tagged PHLDB1 displayed a cytoplasmic disposition in unstimulated cultured adipocytes but translocated to the plasma membrane in response to insulin. Depletion of PHLDB1 by siRNA inhibited insulin stimulation of Akt phosphorylation but not tyrosine phosphorylation of IRS-1. RNAi-based silencing of PHLDB1 in cultured adipocytes also attenuated insulin-stimulated deoxyglucose transport and Myc-GLUT4-EGFP translocation to the plasma membrane, whereas knockdown of the PHLDB1 isoform PHLDB2 failed to attenuate insulin-stimulated deoxyglucose transport. Furthermore, adenovirus-mediated expression of PHLDB1 in adipocytes enhanced insulin-stimulated Akt and p70 S6 kinase phosphorylation, as well as GLUT4 translocation. These results indicate that PHLDB1 is a novel modulator of Akt protein kinase activation by insulin.

Akt protein kinase (also known as protein kinase B) has three isoforms that function as key cellular regulators downstream of various growth factors and hormonal signals (1). A large panel of Akt substrate proteins have been identified that regulate proliferation, growth, survival, and metabolism in many cell types (2). Akt is a member of the large AGC protein kinase family, which includes protein kinase C (PKC), 3-phosphoinositide-dependent kinase 1 (PDK1), Rho-activated kinase, and p70

ribosomal S6 kinase (S6K).<sup>3</sup> Akt is composed of three functionally distinct regions as follows: an N-terminal pleckstrin homology (PH) domain, a central catalytic kinase domain, and a C-terminal hydrophobic motif (3). Akt activation is thought to proceed through its recruitment to the plasma membrane via interaction of its PH domain with the phosphoinositides, specifically PI(3,4,5)P<sub>3</sub> and PI(3,4)P<sub>2</sub> produced by p85/p110 phosphoinositide 3-kinases (PI3K) (4, 5). The lipid-bound Akt is phosphorylated by two protein kinases, PDK1, which is also recruited through its PH domain binding to PI(3,4,5)P<sub>3</sub> and phosphorylates Thr-308 in the activation T-loop of Akt (6), and mammalian target of rapamycin complex 2 (mTORC2) (7), which phosphorylates Akt Ser-473 in the hydrophobic motif. Both phosphorylations are necessary to fully activate the Akt protein kinase (8). The phosphorylated hydrophobic motif of Akt provides a docking site for PDK1 (9–11).

Recently a more detailed “PH-in/PH-out” model for Akt activation has been proposed (12). Förster resonance energy transfer (FRET)/two-photon fluorescence lifetime imaging microscopy suggested that the preactivation complex of Akt and PDK1 is maintained in an inactive state through an Akt intramolecular interaction between its PH domain and kinase domains (PH-in conformer). This domain-domain interaction apparently prevents the Akt activation loop from being phosphorylated by PDK1. Upon stimulation, Akt PH-domain interaction with phosphoinositides and the concomitant change in Akt conformation purportedly cause the separation of the PH domain and kinase domain (PH-out conformer), allowing the associated PDK1 to phosphorylate Akt Thr-308 (13). This model is also consistent with data showing phosphorylation of Akt by PDK1 is associated with membrane recruitment and a conformational change in Akt (14). Akt also contains a turn motif phosphorylation site in the kinase domain (Thr-450 in Akt1, Thr-451 in Akt2, and Thr-447 in Akt3). The mTORC2-dependent phosphorylation of the Akt turn motif is required for kinase stability and may also protect the hydrophobic motif site from dephosphorylation (15–17).

One of the established functions of Akt is to mediate insulin signaling to cause GLUT4 glucose transporter translocation from intracellular membranes to the cell surface membrane,

\* This work was supported, in whole or in part, by National Institutes of Health Grant DK060564 (to M. P. C.). This work was also supported by an American Diabetes Association Junior Faculty Award (to Z. Y. J.).

<sup>‡</sup> Author's Choice—Final version full access.

<sup>1</sup> To whom correspondence may be addressed. E-mail: zjiang@sanfordburnham.org.

<sup>2</sup> To whom correspondence may be addressed. E-mail: Michael.Czech@umassmed.edu.

<sup>3</sup> The abbreviations used are: S6K, S6 kinase; TIRF, total internal reflection fluorescence; PI, phosphatidylinositol.

## Novel Protein PHLDB1 Regulates Akt Activation

thereby stimulating glucose uptake into muscle and adipose tissues (18–20). The aim of this study was to search for new proteins that may function to enhance insulin signaling to Akt and GLUT4 translocation. Here, we report the identification of a novel, uncharacterized protein denoted pleckstrin homology-like domain, family B, member 1 (PHLDB1) that displays such a function. PHLDB1 (also known as LL5 $\alpha$ ) is a protein that was first identified in a bioinformatics screen (21) and has an isoform (PHLDB2/LL5 $\beta$ ) with 70% identity at the protein level containing a Forkhead-associated (FHA) domain and a C-terminal PH domain. LL5 $\beta$  has been suggested to interact with filament C (22, 23), a confirmed direct target of Akt (24). LL5 $\beta$  is also implicated as a binding partner for CLASPs that are mammalian microtubule-stabilizing proteins involved in the interaction between distal microtubule ends and the cell cortex (25). In a screen for synaptically enriched transcripts at the neuromuscular junction, LL5 $\beta$  was identified as a regulator of postsynaptic differentiation and is required for assembly of the postsynaptic apparatus (26). In this study, we found that PHLDB1 is highly expressed in cultured adipocytes and adipose tissues. We also demonstrated that PHLDB1 binds PI(3,4,5)P<sub>3</sub> through its PH domain, functions in adipocytes as a positive regulator of Akt activation, and is required for optimal insulin-induced glucose transport and GLUT4 translocation.

### EXPERIMENTAL PROCEDURES

**Materials**—Human insulin was obtained from Lilly. Rabbit polyclonal antibodies against phospho-Akt/PKB Thr-308, phospho-Akt/PKB Ser-473, total Akt, phospho-p70 S6 kinase (Thr-389), and p70 S6 kinase were from Cell Signaling Technology (Beverly, MA). Rabbit polyclonal antibody against Myc epitope was from Upstate (Charlottesville, VA). Monoclonal antibody HA.11 against HA epitope was from Covance (Emeryville, CA). Goat polyclonal antibody against GLUT4 was from Santa Cruz Biotechnology (Santa Cruz, CA). Rabbit polyclonal antibody against GLUT1 was kindly provided by Dr. Paul Pilch (Boston University). Rabbit polyclonal antibody against mouse PHLDB1 Forkhead-associated domain was generated by Rockland (Gilbertsville, PA).

**Cell Culture and Electroporation of 3T3-L1 Adipocytes**—The 3T3-L1 fibroblasts were grown in DMEM supplemented with 10% FBS, 50  $\mu$ g/ml streptomycin, and 50 units/ml penicillin and differentiated into adipocytes as described previously (20, 27). The 3T3-L1 adipocytes were transfected with siRNA duplexes or cDNA expression constructs by electroporation as described previously (20). Briefly, the adipocytes, on the 4th day of differentiation, were detached from culture dishes with 0.25% trypsin and 0.5 mg of collagenase/ml in PBS, washed twice, and resuspended in PBS. Half of the cells from one 150-mm dish were then mixed with the indicated siRNA duplexes or siRNA smart pools, which were delivered to the cells by a pulse of electroporation with a Bio-Rad gene pulser II system at the setting of 0.18 kV and 950 microfarad capacitance. After electroporation, cells were immediately mixed with fresh media and reseeded into multiple well plates.

**siRNAs and Constructs**—siRNA smart pools and duplexes were synthesized and purified by Dharmacon Research, Inc. (Lafayette, CO), and transfected into the 3T3-L1 adipocytes by

electroporation as described previously (20). The targeting sequences of each gene are as follows: Akt1/PKB $\alpha$ , AACCA-GGACCACGAGAAGCUG; and Akt2/PKB $\beta$ , GAGAGGAC-CUCCAUGUAG and UGCCAUUCUACAACCAGGA. The smart pool siRNAs were used to induce gene-specific silencing of PHLDB1 (M-062345) (the targeting sequence: GAAG-ACCCAUGACCGGUUG, AAAGGAAGCUCACGCAGAG, GAAGUCAAGCUCGGGAAA, and CCUAUUACGUGG-ACAAACA).

For cDNA expression constructs, cDNA clone of mouse PHLDB1 (accession number BC058712) was obtained from the ATCC with clone ID 10699283. Clone was provided in pYX-Asc vector. To make a full-length 3HA-tagged construct, full-length cDNA from the original clone was cut with restriction enzyme BamHI (sites 94 and 5085) and was cloned at right frame by cutting 3HA-tagged CMV vector with BamHI site. For full-length EGFP-PHLDB1, the original cDNA was cut with restriction enzyme BamHI and cloned into pEGFP C3 vector at the BglIII site. Cloning at BglIII made the cDNA of PHLDB1 in a right frame with the GFP tag. For 3HA only and 3HA-PHLDB1 adenovirus constructs, cDNA of either 3HA or 3HA-PHLDB1 was cloned into the molecular clone of E1/E3-deleted human adenovirus serotype 5 vector. The expression of 3HA or 3HA-PHLDB1 was driven by the CMV promoter. AdCMV3HA or AdCMVPHLDB1 vector genome was released from plasmid backbone by PacI digestion and transfected into 293 cells for virus rescue, followed by expansion and purification by the CsCl sedimentation method.

**Affymetrix GeneChip Analysis**—Isolation of RNA and Affymetrix GeneChip analysis was performed as described for 3T3-L1 fibroblasts and adipocytes (28). RNA was prepared from TRIzol (catalogue no. 15596-018, Invitrogen) following the manufacturer's instructions, and cDNA and cRNA were made using Affymetrix One-Cycle cDNA synthesis and IVT labeling kits. cRNA was hybridized to Affymetrix GeneChips MG-U74A, MG-U74B, and MG-U74C or Mouse Expression Set 430 (Mouse 430A and Mouse 430B). All microarray experiments were performed in triplicate using multiple plates of cells.

**Quantitative Real Time PCR**—RNA isolation was performed according to the TRIzol reagent protocol. Briefly, media were aspirated, and the cells were washed once with ice-cold phosphate-buffered saline. Next, 1 ml of TRIzol reagent was added to each well. The concentration and the purity of the RNA were determined by measuring the absorbance at 260/280 nm. To further determine the quality of the RNA, 1 g of total RNA was run on a 1% agarose gel, and the quality of the 28 S and 18 S ribosomal bands was inspected visually. cDNA was synthesized using the iScript cDNA synthesis kit (catalogue no. 170-8891) from Bio-Rad according to the protocol provided by the manufacturer. For real time PCR, cDNA was loaded into the 96-well plate for detection of the specific target genes. Primers used were designed with primer bank (29) as follows: mouse PHLDB1 forward primer GCAGCCAAGAGTC-CGAATCC and reverse primer GGGCCACCATGTAGT-ACAACC and mouse PHLDB2 forward primer AGCCG-CGTTTCTGAAAGCA and reverse primer CATCCGG-CGGTCTTCCATT. Hypoxanthine-guanine phosphoribosyl-

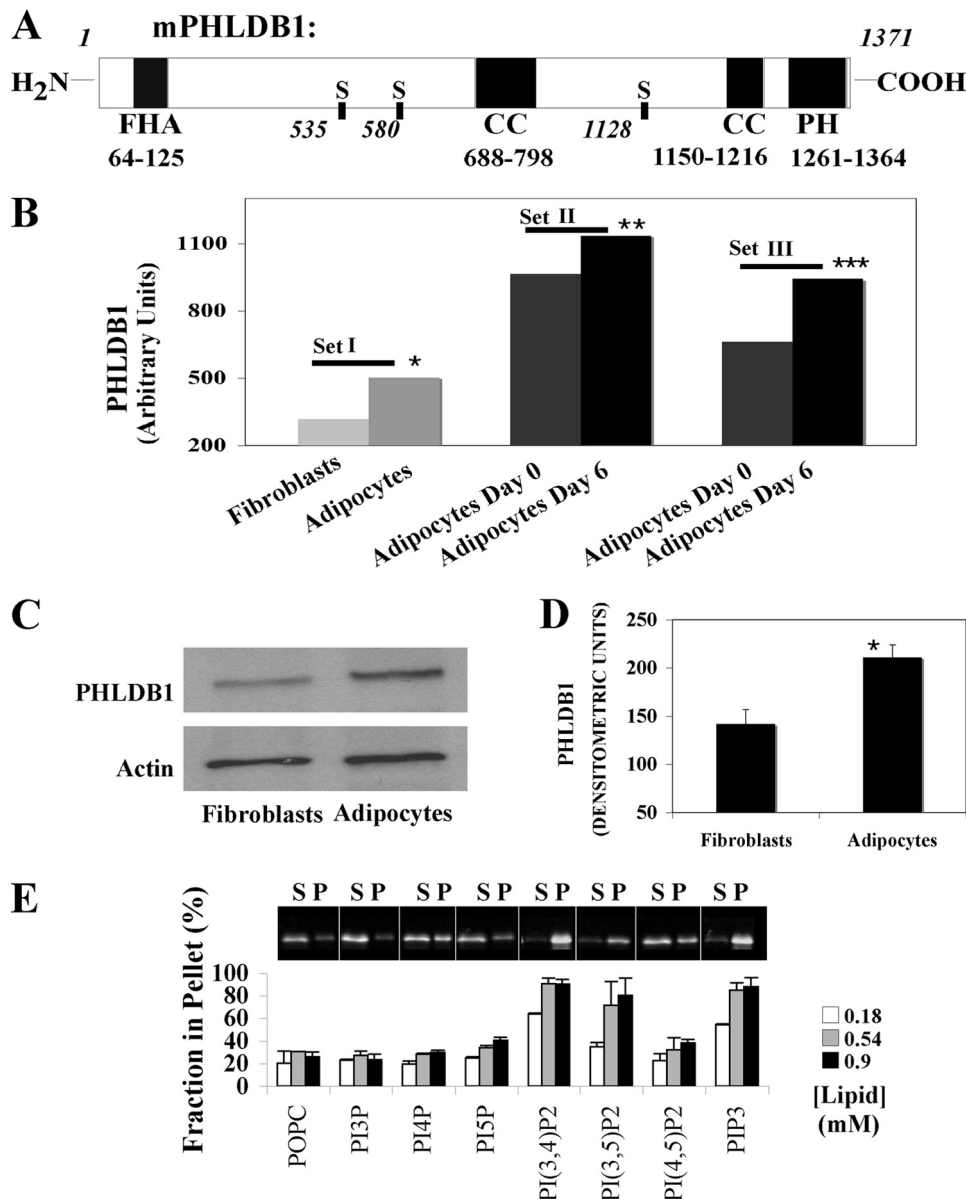


**FIGURE 1. PHLDB1 domain structure and expression profiles.** *A*, schematic shows the domain structure of the PHLDB1 protein. *FHA*, Forkhead-associated domain. *CC*, coiled coil domain. *B*, Affymetrix GeneChip analyses of PHLDB1 expression in fibroblasts and adipocytes. *Set I*, comparison of 3T3-L1 fibroblasts and adipocytes on day 7 post-differentiation. *Sets II* and *III* represent two different probe sets from Affymetrix GeneChip analysis comparing 3T3-L1 adipocytes on day 0 and 6 post-differentiation, respectively. The unpaired Student's *t* test showed the following: \*,  $p < 0.01$ ; \*\*,  $p < 0.001$ ; \*\*\*,  $p < 0.0001$  by comparing 3T3-L1 fibroblasts and adipocytes in the different sets. *C*, Western blot shows 3T3-L1 fibroblast and adipocyte expression of PHLDB1. *D*, protein bands were scanned, and intensities were determined by densitometry using Adobe Photoshop CS2 software. Data are presented as the mean  $\pm$  S.E. of three independent experiments, and the unpaired Student's *t* test showed the following: \*,  $p < 0.01$  by comparing 3T3-L1 fibroblasts and adipocytes. *E*, profile of the phosphoinositide binding specificity of the PHLDB1 PH domain. Binding specificity was measured by incubation and ultracentrifugation of the PHLDB1 PH domain with sucrose-loaded palmitoyl oleoylphosphatidylcholine (POPC) liposomes containing 3% of the indicated phosphoinositides, at three total lipid concentrations. Error bars indicate standard deviation ( $n = 3$ ). Gels above the plot show representative supernatant (S) and pellet (P) fractions for the indicated phosphoinositides at a lipid concentration of 0.9 mM.

transferase was used as an internal loading control. Samples were run on the MyIQ real time PCR system (Bio-Rad). Relative gene knockdown was determined using the *CT* method (30).

**Phosphoinositide Binding Assay**—A construct of PHLDB1 consisting of the C-terminal region PH domain (residues 1233–1371) was amplified with Vent polymerase (New England Biolabs), digested with *Sal*I and *Bam*HI, and ligated into a modified

pET28 vector incorporating an N-terminal His<sub>6</sub>-SUMO fusion. The construct was sequenced and expressed in BL21(DE3)RIPL cells (Stratagene) cultured in 2 $\times$  YT-kan (16 g of tryptone, 10 g of yeast extract, 5 g of NaCl, and 50 mg of kanamycin per liter). Cultures were grown at 37 °C to an *A*<sub>600</sub> of 0.6 and induced with 1 mM isopropyl 1-thio- $\beta$ -D-galactopyranoside for 3 h. Cells were disrupted by sonication in 50 mM Tris (pH 8.0), 0.1% 2-mercaptoethanol, 0.1 mM PMSF, 1 mg/ml lysozyme, and 0.01 mg/ml DNase I. Lysates were supplemented with 0.5% Triton X-100 and centrifuged at 35,000  $\times$  *g* for 1 h. Supernatants were loaded onto nickel-nitrilotriacetic acid columns (GE Healthcare) equilibrated with 50 mM Tris (pH 8.0) and 0.1% 2-mercaptoethanol. The columns were washed with buffer containing 15 mM imidazole and eluted with 300 mM imidazole. PHLDB1 PH domain was further purified by chromatography on HiTrap Q and Superdex-75 (GE Healthcare).

The binding of the PH domain of PHLDB1 to phosphoinositides was measured by using ultracentrifugation of sucrose-loaded liposomes as described previously (35). PHLDB1 PH domain (0.6  $\mu$ M) was incubated with palmitoyl oleoylphosphatidylcholine liposomes containing 3% of one of seven phosphoinositides (PI3P, PI4P, PI5P, PI(3,4)P<sub>2</sub>, PI(3,5)P<sub>2</sub>, PI(4,5)P<sub>2</sub>, and PI(3,4,5)P<sub>3</sub>) for 15 min at 25 °C; liposomes were added to the assays to final lipid concentrations of 0.18, 0.5, and 0.9 mM. Incubation was followed by centrifugation at 100,000  $\times$  *g* for 30 min at 25 °C. Normalized volumes of supernatant and resuspended pellet fractions were analyzed by SDS-PAGE with Krypton™ protein stain (Pierce); bands were visualized using a Kodak Image Station

4000MM and integrated using Image J 1.38X software, following background correction (rolling circle, 200 points).

**Immunoblotting**—After experimental treatments, cell lysates were harvested by the addition of SDS lysis buffer (2% SDS, 30 mM NaCl, 10 mM Hepes (pH 7.4), 20 mM NaF, 1 mM NaPP<sub>i</sub>). For detecting phosphoproteins, cells were starved overnight in serum-free DMEM with 0.5% BSA. Cells were then incubated

## Novel Protein PHLDB1 Regulates Akt Activation

with insulin for 15 min and harvested with 1% SDS lysis buffer as described above. The total cell lysates (20–50  $\mu\text{g}$  of protein) were resolved with SDS-PAGE and electrotransferred to nitrocellulose membranes, which were incubated with primary antibodies. All the membranes were then incubated with appropriate horseradish peroxidase-linked secondary antibodies (1:10,000 dilution each) for 1 h at room temperature. The membranes were washed with wash buffer (PBS (pH 7.4), 0.1% Tween 20) for 1 h at room temperature after incubation with each antibody before detection with ECL<sup>TM</sup> kit.

**Deoxyglucose Uptake Assay**—To detect the effect of specific-gene silencing on insulin-stimulated glucose transport, [<sup>3</sup>H]deoxyglucose uptake assays were carried out in 3T3-L1 adipocytes as described previously (20). Briefly, siRNA-transfected cells were reseeded on 24-well plates and cultured for 72 h before serum starvation for 3 h with Krebs-Ringer Hepes (KRH) buffer (130 mM NaCl, 5 mM KCl, 1.3 mM CaCl<sub>2</sub>, 1.3 mM MgSO<sub>4</sub>, 25 mM Hepes (pH 7.4)) supplemented with 0.5% BSA and 2 mM sodium pyruvate. Cells were then stimulated with insulin for 30 min at 37 °C. Glucose uptake was initiated by addition of 2-[1,2-<sup>3</sup>H]deoxy-D-glucose to a final assay concentration of 100  $\mu\text{M}$  for 5 min at 37 °C. Assays were terminated by four washes with ice-cold KRH buffer, and the cells were solubilized with 0.4 ml of 1% Triton X-100, and <sup>3</sup>H was determined by scintillation counting. Nonspecific deoxyglucose uptake was measured in the presence of 20  $\mu\text{M}$  cytochalasin B and was subtracted from each determination to obtain specific uptake.

**Immunofluorescence Microscopy and Image Analysis**—Unless described otherwise, fluorescence microscopy was carried out with a IX70 inverted microscope (Olympus America, Inc., Melville, NY) with CCD camera (Roper Scientific, Inc., Trenton, NJ). To examine Myc-GLUT4-EGFP translocation in adipocytes transfected with the cDNA, cells after experiment treatments were serum-starved and insulin-stimulated, fixed, and immunostained with anti-Myc monoclonal antibody and Alex Fluor 594 goat anti-mouse IgG (Invitrogen). Images were collected with a 60  $\times$  1.25 numerical aperture oil immersion objective. MetaMorph software (Universal Imaging, West Chester, PA) was used for image processing and quantification. Cells expressing Myc-GLUT4-EGFP were selected manually based upon green fluorescent protein (GFP) fluorescence. The total GFP and Myc fluorescence intensity per cell was calculated, and the average fluorescence intensity per pixel was determined by dividing the total intensity by the area of the cell measured in pixels. To correct for background fluorescence, the same measurements were made for cells that did not express Myc-GLUT4-EGFP. The background fluorescence intensities per pixel (for both the Myc and GFP fluorescence) were subtracted from the experimental data. The Myc/GFP ratio was calculated for each cell and averaged over multiple cells for each experiment.

**TIRF Microscopy and Image Processing**—The custom-built TIRF microscope has been described previously (31). It is built around a commercially available Olympus IX81 inverted microscope with a PlanApo oil, 60 $\times$ , NA1.45 objective. Excitation wavelengths are provided by two Coherent Innova 70C ion lasers, argon (488 nm) and an argon-krypton (568 nm). The

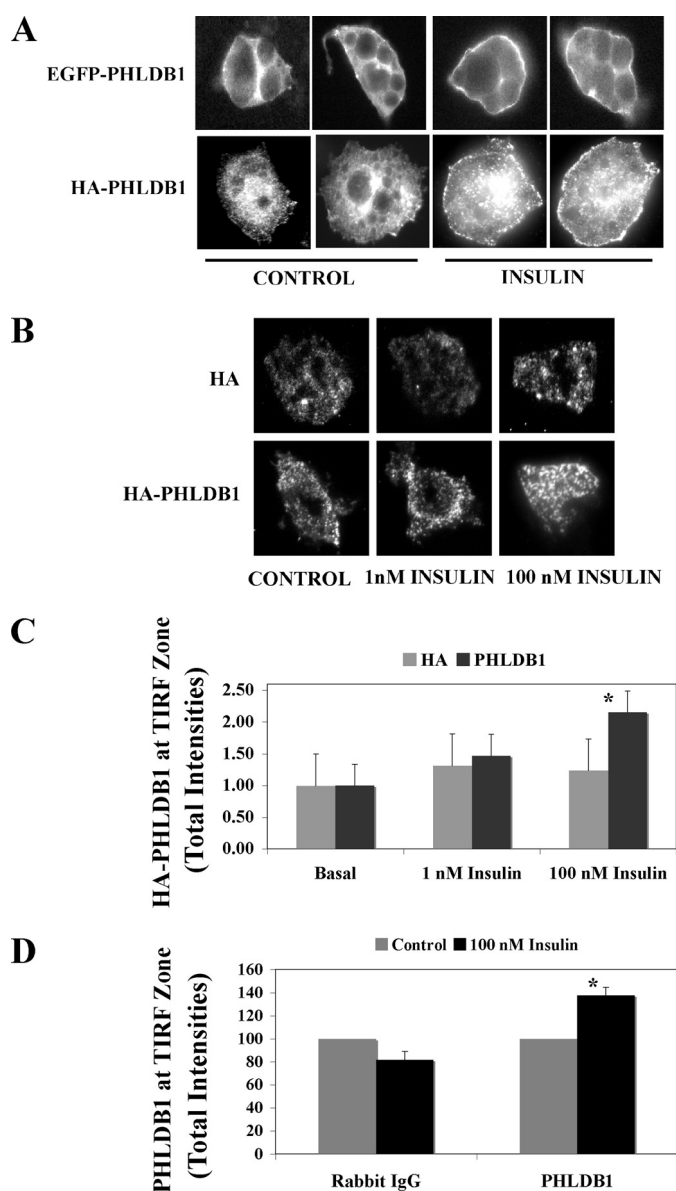


**FIGURE 2. PHLDB1 is a novel insulin-responsive protein.** *A*, day 4 3T3-L1 adipocytes were transfected with 50  $\mu\text{g}$  of EGFP-PHLDB1 or HA-PHLDB1 plasmid DNAs by electroporation. Images of enhanced GFP-positive or HA-positive cells from control and insulin-stimulated groups were obtained using an Olympus IX-70 inverted microscope with a CCD camera as indicated under "Experimental Procedures." *B*, representative TIRF images from control and insulin-stimulated cells were obtained using a custom-built TIRF microscope. *C*, for each condition, the fluorescence intensity of TIRF images within a defined cell boundary was analyzed following correction for background fluorescence using custom-designed software. Data are presented as the mean  $\pm$  S.E. of 360 TIRF images from three separate experiments. Each insulin-stimulated condition was compared with the basal condition using the unpaired Student's *t* test, and significant differences (\*,  $p < 0.05$ ) are noted. *D*, day 4 3T3-L1 adipocytes treated with 100 nM insulin following overnight starvation were immunostained with rabbit antibody against PHLDB1 or rabbit IgG and then the second antibody of 488 goat anti-rabbit IgG. The TIRF images were taken and analyzed as described as above. Data are presented as the means  $\pm$  S.E. of 360 TIRF images from three separate experiments.

original fiber positioning mechanism coupling laser beams into the TIRF illuminator has been replaced by a three-axis translation stage to achieve negligible beam drift during image acquisition. The microscope and critical optics for TIRF illumination are housed in a temperature-controlled chamber to minimize focus drift in the TIRF evanescent field. The camera is a cus-

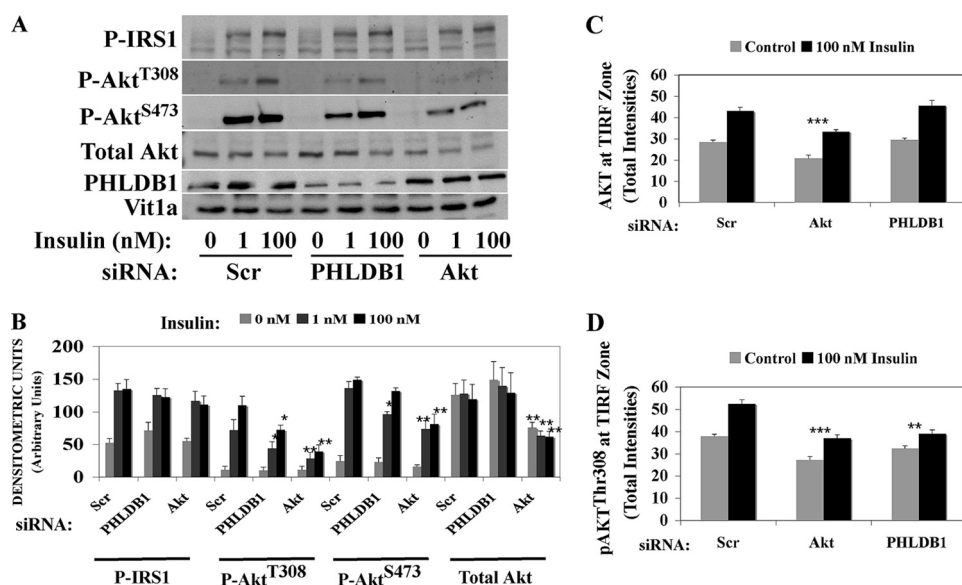


**FIGURE 3. Silencing of PHLDB1 by gene-specific siRNA inhibits Akt phosphorylation.** Day 4 3T3-L1 adipocytes were transfected with 10 nmol of siRNAs as indicated by electroporation. 72 h after re-seeding, adipocytes were starved for 5 h before 1 or 100 nM insulin stimulation. *A*, Western blot shows protein bands detected by different antibodies as indicated. *B*, protein bands were scanned, and intensities were determined by densitometry using Adobe Photoshop CS2 software. Data are presented as the mean  $\pm$  S.E. of five independent experiments, and the unpaired Student's *t* test showed the following: \*,  $p < 0.01$ , and \*\*,  $p < 0.001$ , by comparing PHLDB1 and Akt knockdowns with the scrambled siRNA groups. *C* and *D*, knockdown of PHLDB1 by gene-specific siRNA inhibited insulin-stimulated Akt phosphorylation at the TIRF zone in 3T3-L1 adipocytes. Day 4 3T3-L1 adipocytes were transfected with 10 nmol of siRNAs as indicated by electroporation. Following overnight starvation, cells were stimulated with 100 nM insulin and immunostained for the endogenous Akt (*C*) or pAKT<sup>Thr308</sup> (*D*). TIRF images from control and insulin-stimulated cells were obtained using a custom-built TIRF microscope. For each condition, the fluorescence intensity within a defined cell boundary was analyzed as described above. Data are presented as the means  $\pm$  S.E. of more than 500 TIRF images from three separate experiments, and the *p* values from the unpaired Student's *t* test showed the following: \*\*,  $p < 0.01$ , and \*\*\*,  $p < 0.001$ , by comparing PHLDB1 and Akt knockdowns with the scrambled siRNA groups in the insulin stimulation condition.

tom-built MIT Lincoln Laboratory 640  $\times$  480 element CCD of 24  $\mu$ m pixels, with a quantum efficiency of 80% at 550 nm. Shutters controlling laser illumination and filter wheels selecting excitation and emission wavelengths are synchronized to the camera by an InstruTECH digital and analog interface linked to a computer. The camera acquires 12-bit images and is electronically interfaced to an acquisition system with custom software designed to handle large, fast data flows.

The local Biomedical Imaging Group developed the computer programs for image analysis. Raw CCD images were corrected for black level and dark current. The average intracellular fluorescence intensity, above background, for each image was computed as follows. First, an image was substantially blurred, to create a reasonable estimate of the actual intracellular area from noncontinuous and punctate distributions of fluorescence signal, by taking a moving average of 15  $\times$  15 pixels. The blurred image was then subjected to an intensity threshold to visually exclude extracellular regions and a binary mask constructed. This mask was then applied to its unblurred image, and the mean intensities were computed of those pixels inside the mask (cellular) and those outside the mask (background). The average intensity of that image was computed as the difference of the two.

## RESULTS AND DISCUSSION

**PHLDB1 Identification**—We identified PHLDB1 by searching for proteins that contain at least one PH domain and one or

more Akt substrate phosphorylation motifs from gene profiling databases generated in our laboratory. These databases were described previously (32). PHLDB1 (gene ID NM\_153537) is a 150-kDa protein, and the mouse PHLDB1 has three high stringency Akt phosphorylation sites at Ser-535, Ser-580, and Ser-1128 predicted by ScanSite. It contains a PH domain in the C-terminal region and an Forkhead-associated domain in its N-terminal region in addition to two coiled-coil domains (Fig. 1A).

**PHLDB1 Expression**—Because of limited previous studies of PHLDB1, we first investigated its expression profile. As presented in Fig. 1, upon 3T3-L1 fibroblast differentiation into adipocytes, both mRNA and protein levels of PHLDB1 increased 30–50% based on Affymetrix GeneChip analyses (Fig. 1B) and immunoblot using anti-PHLDB1 antibody (Fig. 1, C and D). PHLDB1 protein was detectable in multiple mouse tissues, including white fat, brown fat, brain, lung, muscle, and heart as indicated by data not shown. The

Genomics Institute of the Novartis Research Foundation Database shows that PHLDB1 is highly expressed in brain and adipose tissues of mice and humans.

**PHLDB1 Binds to PI(3,4)P<sub>2</sub> and PI(3,4,5)P<sub>3</sub>**—PH domains of many proteins have been characterized as motifs that interact with specific phosphoinositol lipids, including species like PI(3,4,5)P<sub>3</sub> generated in response to agonist-stimulated PI3K pathways. The molecular basis by which certain PH domains are able to interact with PI(3,4,5)P<sub>3</sub> has not been established definitively; however, some studies indicated that six conserved residues that lie in the PH domain in a KX-Sma-X<sub>6–11</sub>(R/K)XR-Hyd motif (where X is any amino acid; Sma is a small amino acid, and Hyd is a hydrophobic amino acid) are required for PI(3,4,5)P<sub>3</sub> interaction (33, 34). The PH domain of PHLDB1 possesses such a potential PI(3,4,5)P<sub>3</sub>-binding motif. Thus, to test if the PH domain of PHLDB1 indeed binds to PI(3,4,5)P<sub>3</sub>, we made a His<sub>6</sub>-SUMO fusion protein of the PH domain of PHLDB1 and measured the binding of the fusion protein to phosphoinositides using ultracentrifugation of sucrose-loaded liposomes (35). Increasing concentrations of liposomes containing PI(3,4)P<sub>2</sub> or PI(3,4,5)P<sub>3</sub> resulted in close to 100% partitioning of the protein with the membrane fraction (Fig. 1E). Partitioning with PI(3,5)P<sub>2</sub> was lower, but increased to 80% at the highest lipid concentration. Partitioning with all other phosphatidylinositol phosphates was similar to binding to palmitoylcholine vesicles with between 20 and 30% partitioning to the pellet fraction (Fig. 1E). These

## Novel Protein PHLDB1 Regulates Akt Activation

results indicated that PHLDB1 PH domain binds selectively to both PI(3,4)P<sub>2</sub> and PI(3,4,5)P<sub>3</sub> and suggested that PHLDB1 might respond to agonist-stimulated PI3K signaling pathways.

**PHLDB1 Localization and Insulin Responsiveness**—We next assessed the cellular localization of PHLDB1 and its response to insulin, which generates PI(3,4,5)P<sub>3</sub> at the plasma membrane (36–38). We observed the localization of both HA- and GFP-tagged PHLDB1 in serum-starved and insulin-treated 3T3-L1 adipocytes (Fig. 2). Under basal conditions, PHLDB1 distributes throughout the cytoplasm, concentrated in the perinuclear region. Treatment of cells with insulin results in increased detection of PHLDB1 in the periphery of the cells suggesting plasma membrane translocation (Fig. 2A). To verify this apparent movement to the plasma membrane, we used total internal reflection fluorescence (TIRF) microscopy to observe and quantitate PHLDB1 translocation (Fig. 2, B and C). Upon treatment with 100 nM insulin, detection of HA-PHLDB1 in the TIRF zone (within ~100 nm of the cell surface) increased significantly. Under these conditions, detection of HA alone did not change. We also observed a 35% increase of endogenous PHLDB1 protein into the TIRF zone upon insulin stimulation using anti-PHLDB1 antibody (Fig. 2D). Live cell TIRF microscopy indicates high concentrations of EGFP-PHLDB1 located in membrane ruffles upon insulin stimulation (data not shown), a known site of insulin stimulated PI(3,4,5)P<sub>3</sub> accumulation (39). These results suggest that PHLDB1 translocates to the plasma membrane upon insulin stimulation, consistent with intracellular targeting of the protein via a PI(3,4,5)P<sub>3</sub>-binding PH domain. EGFP-PHLDB1 translocation from cytoplasm to cell membrane by insulin stimulation was inhibited by PI3K inhibitor wortmannin (data not shown).

**Silencing of PHLDB1 Expression Inhibits Akt Phosphorylation**—Translocation of PHLDB1 to the plasma membrane in response to insulin prompted us to investigate potential roles of the protein in insulin-signaling pathways. Early events of insulin signaling known to include activation of the insulin receptor, tyrosine phosphorylation of insulin receptor substrate (IRS) proteins, and recruitment and activation of PI3K result in activation of Akt phosphorylation (40). We applied gene-specific siRNA knockdown to investigate the role of PHLDB1 in this cascade (Fig. 3). Transfection of PHLDB1-specific siRNAs into 3T3-L1 adipocytes caused ~75% reduction in the PHLDB1 protein. This knockdown has no effect on IRS-1 phosphorylation or total Akt levels. However, decreasing PHLDB1 expression inhibited Akt phosphorylation induced by 1 nM insulin on Thr-308 and Ser-473 by 39 and 29%, respectively, and with 100 nM insulin, the inhibition of PHLDB1 knockdown on Akt phosphorylation on Thr-308 and Ser-473 was 35 and 15%, respectively (Fig. 3, A and B). TIRF microscopy further confirmed that knockdown of PHLDB1 inhibited Akt phosphorylation at the cell membrane without changing total Akt levels (Fig. 3, C and D). These results suggest that PHLDB1 plays a role in Akt activation downstream of insulin receptor activation.

**Overexpression of PHLDB1 Increases Akt and p70S6K Phosphorylation**—Based on the result of PHLDB1 knockdown, we predicted that its overexpression would have the opposite effect, *i.e.* enhancement of insulin-stimulated Akt phosphorylation. We used adenovirus-mediated expression to increase

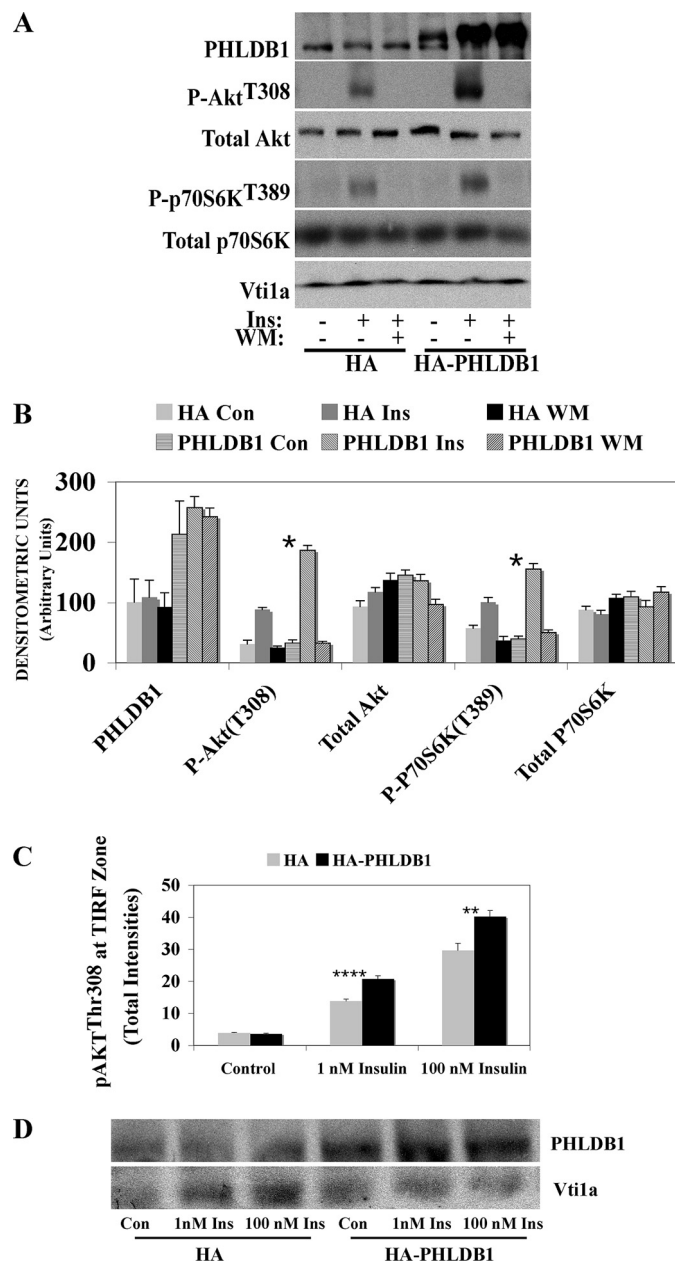


**FIGURE 4. Adenovirus-mediated expression of HA-tagged PHLDB1 enhances insulin-stimulated Akt and p70S6K phosphorylations and GLUT4 translocation at the TIRF zone in 3T3-L1 adipocytes.** Day 4 3T3-L1 adipocytes were infected with 100  $\mu$ l ( $4.7 \times 10^{12}$  particles/ml) of HA control (Con) or HA-PHLDB1 virus particles per  $1 \times 10^9$  cells for 48 h. Following overnight starvation, cells were treated with or without 100 nM wortmannin (WM) and 100 nM insulin (Ins). A, protein bands were scanned, and intensities were determined by densitometry using Adobe Photoshop CS2 software (B). Data are presented as the means  $\pm$  S.E. of three independent experiments and the unpaired Student's *t* test showed the following: \*,  $p < 0.005$ , by comparing the samples from cells overexpressed HA-PHLDB1 with the samples from cells overexpressed HA control viruses. C and D, increase of PHLDB1 protein expression (D) enhanced insulin-stimulated Akt phosphorylation at the TIRF zone in 3T3-L1 adipocytes (C). Day 4 3T3-L1 adipocytes were infected with 10  $\mu$ l ( $2.3 \times 10^{12}$  particles/ml) of HA control or HA-PHLDB1 virus particles per  $6 \times 10^5$  cells for 48 h. Following overnight starvation, cells were stimulated with insulin and immunostained for the endogenous pAKT<sup>Thr-308</sup>. The cells were then imaged with the TIRF microscope and analyzed as described above. Data are presented as the mean  $\pm$  S.E. of more than 720 TIRF images from three separate experiments, and the *p* values from the unpaired Student's *t* test showed the following: \*\*,  $p < 0.01$ , and \*\*\*\*,  $p < 0.0001$ , by comparing the samples from cells overexpressed HA-PHLDB1 with the samples from cells overexpressed HA control viruses.

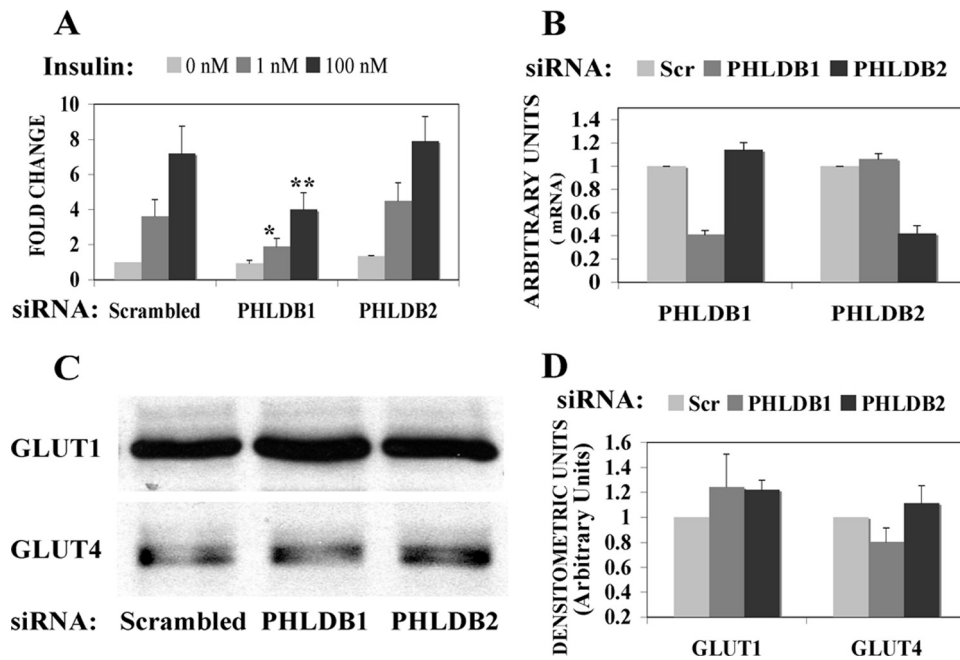


**FIGURE 5. Silencing of PHLDB1 by gene-specific siRNA inhibits insulin-stimulated glucose uptake in 3T3-L1 adipocytes.** Day 4 3T3-L1 adipocytes were transfected with 10 nmol of siRNAs as indicated by electroporation and cultured for 72 h. *A*, comparison of insulin-stimulated glucose uptake by 2-deoxyglucose uptake assay in adipocytes transfected with different siRNAs. Data shown are the means  $\pm$  S.E. of seven independent experiments and the unpaired Student's *t* test showed the following: \*,  $p < 0.01$ , and \*\*,  $p < 0.001$ , indicated by comparing PHLDB1 with the scrambled siRNA groups. *B*, real time PCR analysis of PHLDB1 and PHLDB2 mRNAs levels. Data shown are the means  $\pm$  S.E. of three independent experiments. *C*, Western blot shows GLUT1 and GLUT4 protein levels in 3T3-L1 adipocytes transfected with siRNAs as indicated. *D*, protein bands were scanned, and intensities were determined by densitometry using Adobe Photoshop CS2 software. Data are presented as the means  $\pm$  S.E. of three independent experiments.

PHLDB1 protein levels by about 2-fold in 3T3-L1 adipocytes. Consistent with our prediction, this enhanced Akt Thr-308 phosphorylation by 85% (Fig. 4). To verify that this coincided with enhanced Akt kinase activity, we assessed the result of PHLDB1 expression on phosphorylation of one of the downstream targets of Akt, p70S6K. Increased PHLDB1 protein levels enhanced p70S6K phosphorylation on Thr-389 by 56%. Increasing PHLDB1 protein levels did not induce notable changes to total Akt and p70S6K protein levels (Fig. 4, *A* and *B*). High expression of PHLDB1 also significantly increased Akt phosphorylation on Thr-308 at the cell membrane in 3T3-L1 adipocytes as shown by TIRF microscopy (Fig. 4, *C* and *D*).

**PHLDB1 Affects Insulin-stimulated Glucose Transport**—Insulin stimulates glucose transport in adipocytes via a PI3K/Akt-dependent pathway that results in the translocation of the glucose transporter GLUT4 to the cell surface. Thus, we expected that modulation of Akt activity by PHLDB1 would result in altered glucose uptake in response to insulin. To test this, 3T3-L1 adipocytes were transfected with gene-specific siRNA against PHLDB1 or the closely related protein PHLDB2, an isoform of PHLDB1, which contains a PH domain also reported to bind PI(3,4,5)P<sub>3</sub> (22). These conditions reduced mRNA expression of both genes by  $\sim$ 60% (Fig. 5*B*). Knockdown of PHLDB1 significantly decreased glucose uptake at both 1 and 100 nM doses of insulin, although knockdown of PHLDB2 had no significant effect (Fig. 5*A*). This alteration in glucose transport was not due to altered glucose transporter expression because there was no effect of PHLDB1 knockdown on either GLUT4 or GLUT1 protein levels (Fig. 5, *C* and *D*).

The insulin-stimulated increase in glucose transport in adipocytes is thought to result largely from increased translocation of GLUT4 from an intracellular pool to the plasma membrane. This translocation is dependent on Akt activation; thus we used several approaches to assess the influence of PHLDB1 on this process. We used a dual-tagged GLUT4 construct, EGFP-GLUT4-Myc, in which the Myc epitope tag is within the exofacial loop of GLUT4 (41). Thus, total GLUT4 can be measured by GFP fluorescence, whereas cell surface translocation of GLUT4 can be monitored by Myc antibody staining of nonpermeabilized cells. Insulin treatment of transfected adipocytes results in an  $\sim$ 3-fold increase in Myc/GFP fluorescence ratio (Fig. 6, *A* and *B*) indicative of translocation of the reporter molecule. RNAi-based silencing of PHLDB1 in cultured 3T3-L1 adipocytes (Fig. 6, *C* and *D*) attenuated 0.1 nM insulin-induced Myc-GLUT4-EGFP translocation measured by this method by 43% as shown in Fig. 6*B*. Under these conditions, knockdown of Akt resulted in similar attenuation of Myc-GLUT4-EGFP translocation consistent with the notion that effects of PHLDB1 are exerted via Akt.

We also employed TIRF microscopy to detect endogenous GLUT4 translocation in 3T3-L1 adipocytes. Insulin has been shown to increase GLUT4 detection in the TIRF zone as a result of its translocation from intracellular locations distant from the plasma membrane, *i.e.* outside the region of TIRF illumination (42, 43). Knockdown of PHLDB1 decreased effects of 1 and 100 nM insulin on endogenous GLUT4 translocation about 32 and 36%, respectively (Fig. 6, *E* and *F*). Similar reductions in TIRF zone GLUT4 were observed upon silencing of Akt. We did not observe any morphological changes of actin filaments when PHLDB1 was silenced in basal or insulin-stimulated conditions (Fig. 6*G*). Because expression of PHLDB1 increased Akt activation (Fig. 4), we also tested effects of its expression on GLUT4 translocation. HA-PHLDB1 was expressed by adenovirus infection of 3T3-L1 adipocytes, and the endogenous GLUT4 within the TIRF zone was measured. Increased PHLDB1 expression significantly enhanced insulin-stimulated endogenous GLUT4 translocation to the cell membrane compared with control cells infected with HA adenovirus (Fig. 6, *H* and *I*).

Taken together, these results suggest that the PH domain containing protein PHLDB1 is a novel insulin signaling component and is involved in the regulation of Akt activation and its downstream signaling in adipocytes. The levels of PHLDB1 protein influence a major biological effect of insulin in adipo-

## Novel Protein PHLDB1 Regulates Akt Activation

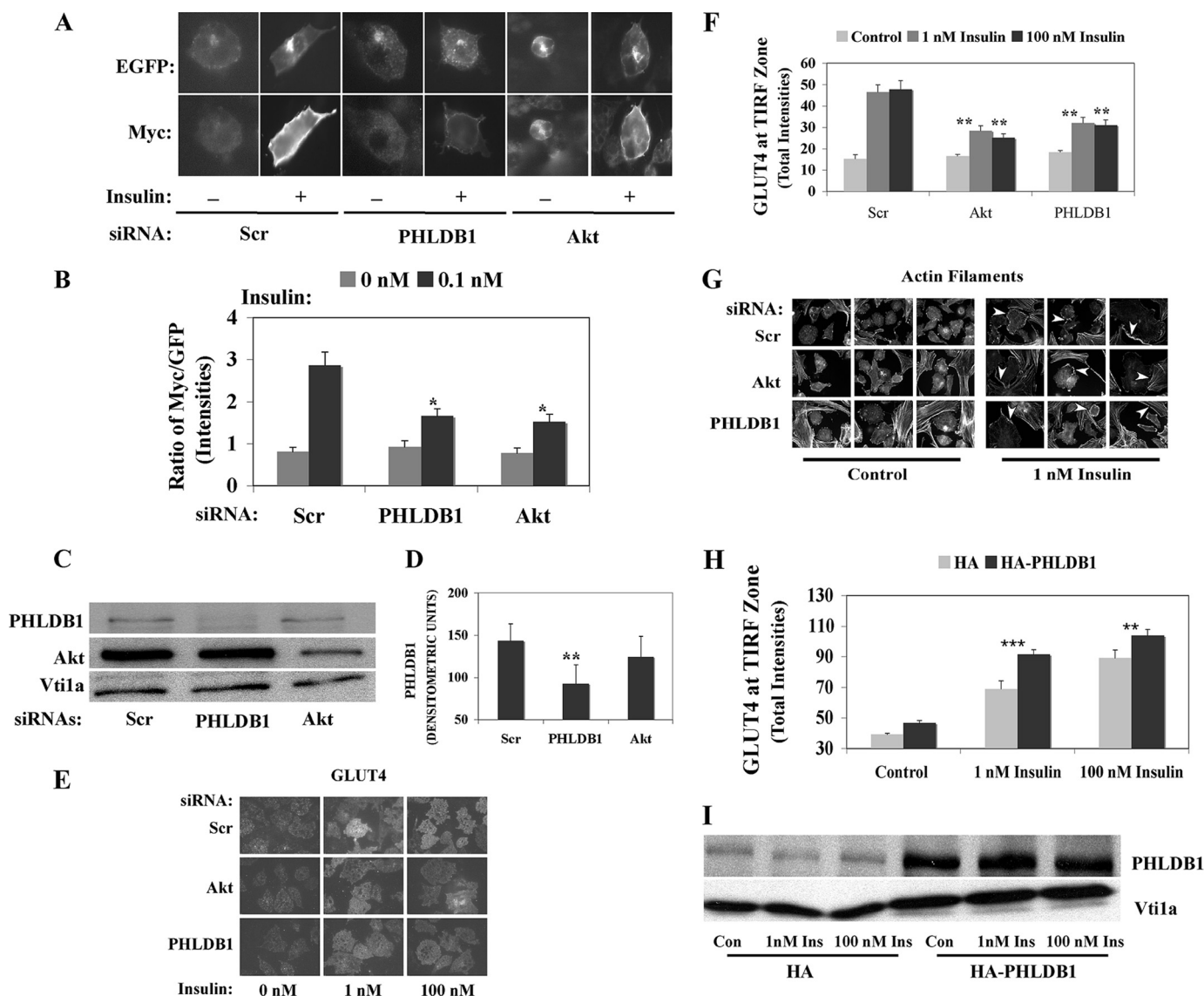


**FIGURE 6. PHLDB1 modulates insulin-stimulated GLUT4 translocation.** 3T3-L1 adipocytes were transfected with 50  $\mu$ g of Myc-GLUT4-EGFP plasmid DNA and 10 nmol of siRNAs as indicated by electroporation. Myc-GLUT4-EGFP translocation to the cell surface in GFP-positive cells was detected with a mouse anti-Myc epitope primary antibody and Alex Fluor 594 goat anti-mouse IgG. *A*, representative images for GFP-positive cells and exofacial Myc staining were obtained using an Olympus IX-70 inverted microscopy with a CCD camera. *B*, average of the total fluorescence intensity and the ratio of Myc to enhanced GFP were determined using MetaMorph software. Data are presented as the means  $\pm$  S.E. of 470 cells analyzed, and the unpaired Student's *t* test showed the following: \*,  $p < 0.01$  by comparing PHLDB1 or Akt with the scrambled siRNA groups. *C*, Western blot shows PHLDB1 and Akt protein levels in 3T3-L1 adipocytes transfected with siRNAs as indicated. *D*, protein bands were scanned, and intensities were determined by densitometry using Adobe Photoshop CS2 software program. Data are presented as the means  $\pm$  S.E. of three independent experiments, and the unpaired Student's *t* test showed the following: \*\*,  $p < 0.001$ , by comparing PHLDB1 with the scrambled siRNA groups. *E* and *F*, knockdown of PHLDB1 by gene-specific siRNA inhibited the translocation of endogenous GLUT4 to TIRF zone. Endogenous GLUT4 was detected with goat anti-GLUT4 primary antibody and Alex Fluor 488-conjugated donkey anti-goat IgG. *E*, representative TIRF images of endogenous GLUT4 from control and insulin-stimulated cells were obtained using a custom-built TIRF microscope. *F*, average of total fluorescence intensities was analyzed with custom-designed software as described above. Data are presented as the means  $\pm$  S.E. of more than 500 TIRF images from three separate experiments, and the unpaired Student's *t* test showed the following: \*\*,  $p < 0.001$ , by comparing PHLDB1 and Akt knockdowns with the scrambled siRNA groups. *G*, representative images of actin filaments detected by rhodamine-phalloidin from control or insulin-stimulated cells were obtained as described above and indicated no changes of actin filaments organizations by knocking down of PHLDB1 (white arrows). *H* and *I*, overexpression of PHLDB1 by adenovirus increased the translocation of endogenous GLUT4 to TIRF zone. Day 4 3T3-L1 adipocytes were infected with 10  $\mu$ l (2.3  $\times 10^{12}$  particles/ml) of HA control or HA-PHLDB1 virus particles per 6  $\times 10^5$  cells for 48 h. Following overnight starvation, cells were stimulated with 1 or 100 nM insulin and immunostained for the endogenous GLUT4. The cells were then imaged with the TIRF microscope and analyzed as described above. Data are presented as the means  $\pm$  S.E. of more than 720 TIRF images from three separate experiments, and the unpaired Student's *t* test showed the following: \*\*,  $p < 0.01$ , and \*\*\*,  $p < 0.001$ , by comparing HA- and HA-PHLDB1-overexpressed cell groups.

cytes, GLUT4 translocation and glucose uptake. These effects appear to be exerted at the level of Akt activation downstream of the IR-IRS1-PI3K pathway activated by insulin. This notion is supported by similar effects of Akt silencing on insulin-stimulated GLUT4 translocation and glucose uptake. The mecha-

nism by which PHLDB1 regulates Akt activation is currently an open question; however, one possibility is that this mechanism is dependent on PHLDB1 recruitment to the cell membrane via its PI(3,4,5)P<sub>3</sub> binding PH domain. Current work in our laboratory is focused on this hypothesis.

*Acknowledgments*—We thank Karl D. Bellve, Clive Standley, and Lawrence M. Lifshitz from the Biomedical Imaging Group at University of Massachusetts Medical School for the support with the TIRF microscopy and imaging analysis. We thank Paul S. Furcinitti from Digital Imaging Core Facility for the support with the immunofluorescence microscopy.

## REFERENCES

- Gonzalez, E., and McGraw, T. E. (2009) *Cell Cycle* **8**, 2502–2508
- Manning, B. D., and Cantley, L. C. (2007) *Cell* **129**, 1261–1274
- Pearce, L. R., Komander, D., and Alessi, D. R. (2010) *Nat. Rev. Mol. Cell Biol.* **11**, 9–22
- Thomas, C. C., Deak, M., Alessi, D. R., and van Aalten, D. M. (2002) *Curr. Biol.* **12**, 1256–1262
- Milburn, C. C., Deak, M., Kelly, S. M., Price, N. C., Alessi, D. R., and Van Aalten, D. M. (2003) *Biochem. J.* **375**, 531–538
- Alessi, D. R., James, S. R., Downes, C. P., Holmes, A. B., Gaffney, P. R., Reese, C. B., and Cohen, P. (1997) *Curr. Biol.* **7**, 261–269
- Sarbassov, D. D., Guertin, D. A., Ali, S. M., and Sabatini, D. M. (2005) *Science* **307**, 1098–1101
- Alessi, D. R., Andjelkovic, M., Caudwell, B., Cron, P., Morrice, N., Cohen, P., and Hemmings, B. A. (1996) *EMBO J.* **15**, 6541–6551
- Balendran, A., Biondi, R. M., Cheung, P. C., Casamayor, A., Deak, M., and Alessi, D. R. (2000) *J. Biol. Chem.* **275**, 20806–20813
- Frödin, M., Antal, T. L., Dümmler, B. A., Jensen, C. J., Deak, M., Gammelt-oft, S., and Biondi, R. M. (2002) *EMBO J.* **21**, 5396–5407
- Biondi, R. M., Kieloch, A., Currie, R. A., Deak, M., and Alessi, D. R. (2001) *EMBO J.* **20**, 4380–4390
- Calleja, V., Alcor, D., Laguerre, M., Park, J., Vojnovic, B., Hemmings, B. A., Downward, J., Parker, P. J., and Larijani, B. (2007) *PLoS Biol.* **5**, e95
- Calleja, V., Laguerre, M., Parker, P. J., and Larijani, B. (2009) *PLoS Biol.* **7**, e17
- Calleja, V., Laguerre, M., and Larijani, B. (2009) *J. Chem. Biol.* **2**, 11–25
- Hauge, C., Antal, T. L., Hirschberg, D., Doehn, U., Thorup, K., Idrissova, L., Hansen, K., Jensen, O. N., Jørgensen, T. J., Biondi, R. M., and Frödin, M. (2007) *EMBO J.* **26**, 2251–2261
- Ikenoue, T., Inoki, K., Yang, Q., Zhou, X., and Guan, K. L. (2008) *EMBO J.* **27**, 1919–1931
- Facchinetti, V., Ouyang, W., Wei, H., Soto, N., Lazorchak, A., Gould, C., Lowry, C., Newton, A. C., Mao, Y., Miao, R. Q., Sessa, W. C., Qin, J., Zhang, P., Su, B., and Jacinto, E. (2008) *EMBO J.* **27**, 1932–1943
- Kohn, A. D., Summers, S. A., Birnbaum, M. J., and Roth, R. A. (1996) *J. Biol. Chem.* **271**, 31372–31378
- Cho, H., Mu, J., Kim, J. K., Thorvaldsen, J. L., Chu, Q., Crenshaw, E. B., 3rd, Kaestner, K. H., Bartolomei, M. S., Shulman, G. I., and Birnbaum, M. J. (2001) *Science* **292**, 1728–1731
- Jiang, Z. Y., Zhou, Q. L., Coleman, K. A., Chouinard, M., Boese, Q., and Czech, M. P. (2003) *Proc. Natl. Acad. Sci. U.S.A.* **100**, 7569–7574
- Katoh, M., and Katoh, M. (2003) *Int. J. Oncol.* **23**, 1477–1483
- Paranavitane, V., Coadwell, W. J., Eguinoa, A., Hawkins, P. T., and Stephens, L. (2003) *J. Biol. Chem.* **278**, 1328–1335
- Paranavitane, V., Stephens, L. R., and Hawkins, P. T. (2007) *Cell. Signal.* **19**, 817–824
- Murray, J. T., Campbell, D. G., Peggie, M., Mora, A., Alfonso, M., and Cohen, P. (2004) *Biochem. J.* **384**, 489–494
- Lansbergen, G., Grigoriev, I., Mimori-Kiyosue, Y., Ohtsuka, T., Higa, S., Kitajima, I., Demmers, J., Galjart, N., Houtsmuller, A. B., Grosveld, F., and Akhmanova, A. (2006) *Dev. Cell* **11**, 21–32
- Kishi, M., Kummer, T. T., Eglen, S. J., and Sanes, J. R. (2005) *J. Cell Biol.* **169**, 355–366
- Harrison, S. A., Buxton, J. M., Clancy, B. M., and Czech, M. P. (1990) *J. Biol. Chem.* **265**, 20106–20116
- Wilson-Fritch, L., Burkart, A., Bell, G., Mendelson, K., Leszyk, J., Nicoloso, S., Czech, M., and Corvera, S. (2003) *Mol. Cell. Biol.* **23**, 1085–1094
- Wang, X., and Seed, B. (2003) *Nucleic Acids Res.* **31**, e154
- Livak, K. J., and Schmittgen, T. D. (2001) *Methods* **25**, 402–408
- Bellve, K. D., Leonard, D., Standley, C., Lifshitz, L. M., Tuft, R. A., Hayakawa, A., Corvera, S., and Fogarty, K. E. (2006) *J. Biol. Chem.* **281**, 16139–16146
- Powelka, A. M., Seth, A., Virbasius, J. V., Kiskinis, E., Nicoloso, S. M., Guilherme, A., Tang, X., Straubhaar, J., Cherniack, A. D., Parker, M. G., and Czech, M. P. (2006) *J. Clin. Invest.* **116**, 125–136
- Isakoff, S. J., Cardozo, T., Andreev, J., Li, Z., Ferguson, K. M., Abagyan, R., Lemmon, M. A., Aronheim, A., and Skolnik, E. Y. (1998) *EMBO J.* **17**, 5374–5387
- Dowler, S., Currie, R. A., Campbell, D. G., Deak, M., Kular, G., Downes, C. P., and Alessi, D. R. (2000) *Biochem. J.* **351**, 19–31
- Buser, C. A., and McLaughlin, S. (1998) *Methods Mol. Biol.* **84**, 267–281
- Whitman, M., Downes, C. P., Keeler, M., Keller, T., and Cantley, L. (1988) *Nature* **332**, 644–646
- Auger, K. R., Serunian, L. A., Soltoff, S. P., Libby, P., and Cantley, L. C. (1989) *Cell* **57**, 167–175
- Ruderman, N. B., Kapeller, R., White, M. F., and Cantley, L. C. (1990) *Proc. Natl. Acad. Sci. U.S.A.* **87**, 1411–1415
- Czech, M. P. (2003) *Annu. Rev. Physiol.* **65**, 791–815
- Lizcano, J. M., and Alessi, D. R. (2002) *Curr. Biol.* **12**, R236–238
- Jiang, Z. Y., Chawla, A., Bose, A., Way, M., and Czech, M. P. (2002) *J. Biol. Chem.* **277**, 509–515
- Lizunov, V. A., Matsumoto, H., Zimmerberg, J., Cushman, S. W., and Frolov, V. A. (2005) *J. Cell Biol.* **169**, 481–489
- Huang, S., Lifshitz, L. M., Jones, C., Bellve, K. D., Standley, C., Fonseca, S., Corvera, S., Fogarty, K. E., and Czech, M. P. (2007) *Mol. Cell. Biol.* **27**, 3456–3469